scientific reports

OPEN

A new obligate CXCL4–CXCL12 heterodimer for studying chemokine heterodimer activities and mechanisms

Khanh T.P. Nguyen[1], Brian Volkman[2], Didier Dréau[1] & Irina V. Nesmelova[3,4][✉]

Chemokines form a family of proteins with critical roles in many biological processes in health and disease conditions, including cardiovascular, autoimmune diseases, infections, and cancer. Many chemokines engage in heterophilic interactions to form heterodimers, leading to synergistic activity enhancement or reduction dependent on the nature of heterodimer-forming chemokines. In mixtures, different chemokine species with diverse activities coexist in dynamic equilibrium, leading to the observation of their combined response in biological assays. To overcome this problem, we produced a non-dissociating CXCL4–CXCL12 chemokine heterodimer OHD_{4-12} as a new tool for studying the biological activities and mechanisms of chemokine heterodimers in biological environments. Using the OHD_{4-12}, we show that the CXCL4–CXCL12 chemokine heterodimer inhibits the CXCL12-driven migration of triple-negative MDA-MB-231 breast cancer cells. We also show that the CXCL4–CXCL12 chemokine heterodimer binds and activates the CXCR4 receptor.

Chemokine signaling is essential in normal physiologic and pathological conditions[1,2]. Chemokine signaling is mediated by intermolecular interactions with G protein-coupled receptors (GPCRs), cell surface glycosaminoglycans (GAGs), and through chemokine homooligomerization[3,4]. Additionally, different chemokines can interact with each other to form heterodimers. These heterophilic interactions have been directly detected by several methods, including co-immunoprecipitation and ligand blot[5–12], surface plasmon resonance[9,11], mass spectrometry[8,13], and NMR (Nuclear Magnetic Resonance) spectroscopy[9,12–17]. A pairwise bidirectional immunoblot chemokine screening shows that heterophilic interactions are abundant in the chemokine family identifying approximately 200 distinct interactions[12].

The role of heterophilic interactions in chemokine signaling remains to be understood. However, it is established that cell responses to chemokine mixtures differ from individual chemokines[18–24]. Treatment with chemokine mixtures demonstrated either a synergistically enhanced or a reduced activity dependent on the microenvironment and the nature of heterodimer-forming chemokines tested[6,7,11,12,15,16,19,22,23,25]. For example, the heterodimerization of platelet-derived CXCL4 with CXCL8 chemokine inhibits the activation and proliferation of endothelial cells, and the CXCL8-induced migration of cells transfected with the CXCR2 chemokine receptor[14,15], whereas CXCL4-CCL5 chemokine heterodimerization promotes the arrest of CCL5-stimulated monocytes on activated endothelium[11]. In addition, chemokines CXCL10 and CCL22, co-expressed in the inflamed skin, synergistically enhance the CCR4-mediated chemotaxis of T cells[25]. Likewise, CCR7 chemokine ligands CCL19 and CCL21 enhance monocytes recruitment by forming heterodimers with CCL7 and CCL2[22], while heterodimers formed by CXCL9 and CXCL12 chemokines co-expressed in the perivascular area of the tumor enhance CXCR4-mediated recruitment of tumor-infiltrating lymphocytes and malignant B cells[6].

The in vivo co-localization, particularly near GAGs, produces favorable conditions for chemokine heterodimerization. In fact, a few studies have already demonstrated the relevance of the heterophilic interactions in in vivo animal models and the possibility of targeting such interactions for therapeutic benefit[9,12,26]. For example, the disruption of the CCL5-CXCL4 heterodimer decreased the CCL5-mediated neutrophil influx, edema formation, and destruction of lung tissue in acute lung injury[26] and attenuated monocyte recruitment, thereby reducing

[1]Department of Biological Sciences, University of North Carolina, Charlotte, NC, USA. [2]Department of Biochemistry, Medical College of Wisconsin, Milwaukee, WI, USA. [3]Department of Physics and Optical Sciences, University of North Carolina, Charlotte, NC, USA. [4]School of Data Science, University of North Carolina, Charlotte, NC, USA. [✉]email: Irina.Nesmelova@uncc.edu
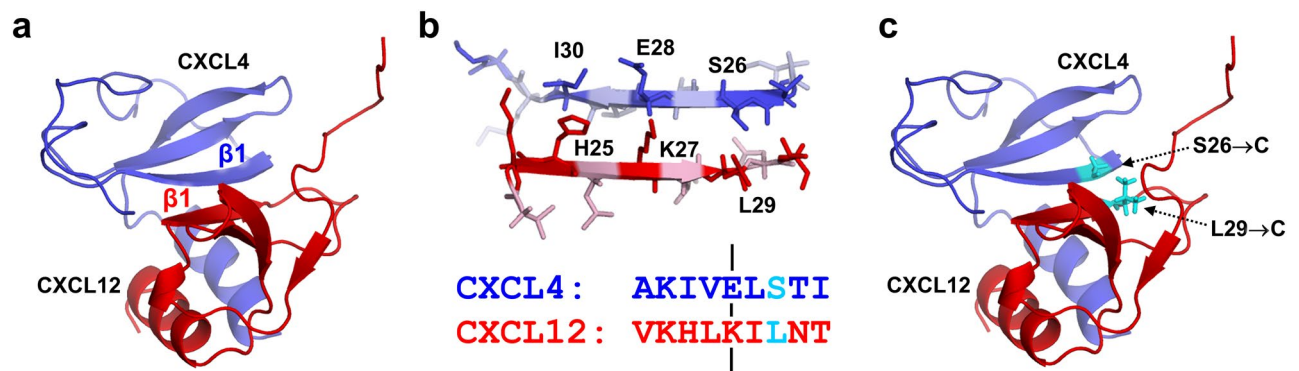
Figure 1. (**a**) Structural model of the CXCL4–CXCL12 heterodimer. The CXCL4 monomer is shown in blue and the CXCL12 monomer is shown in red. First beta-strands forming the intermonomer interface are labeled. (**b**) The structure (top) and the amino acid sequences (bottom) of first beta-strands from CXCL4 (blue) and CXCL12 (red), representing the intermonomer interface, where several amino acids with side chains on the same side of beta-strands are labeled. The axis of symmetry is indicated by black lines on the amino acid sequences of shown beta-strands, and residues selected for mutation are colored in cyan. (**c**) Structural model of the CXCL4–CXCL12 heterodimer with amino acid residues selected for mutation labeled.

atherosclerosis in mice[9]. However, the use of heterophilic interactions as drug targets requires an understanding of the mechanism of action of chemokine heterodimers, which is currently lacking.

In chemokine mixtures, competing homophilic and heterophilic interactions lead to the equilibrium coexistence of different chemokine species including monomers, dimers, heterodimers, and, in some cases, higher-order oligomers (reviewed in[27,28]). The measured biological outcomes represent the combined response to chemokine species, rendering the direct functional assessment of the heterodimer biological activity challenging. Here, we overcome this limitation by generating a new, non-dissociating heterodimer of CXCL4 (platelet factor 4) and CXCL12 (stromal cell-derived factor-1) chemokines, OHD$_{4-12}$ (Obligate HeteroDimer CXCL4–CXCL12). CXCL4 and CXCL12 are both stored and released upon stimulation of platelets[29], thus having ample opportunities to interact in vivo and modulate cell responses in chemokine-rich microenvironments. We also provide proof-of-principle evidence that OHD$_{4-12}$ is a valuable tool for investigating the biological activities and the mechanism of action of the CXCL4–CXCL12 chemokine heterodimer. In particular, we show that the OHD$_{4-12}$ binds and activates the CXCL12 receptor CXCR4 and inhibits the CXCL12-driven migration of MDA-MB-231 breast cancer cells. The mechanistic insight obtained from using the OHD$_{4-12}$ may extend to other chemokine heterodimers and inform experiments testing their mode of action.

Results

Design and production of the obligate CXCL4–CXCL12 heterodimer OHD$_{4-12}$.
Our previous results showed that CXCL4 and CXCL12 chemokines formed heterodimers in in vitro biophysical conditions and in vivo in human platelets[8]. Using experimental NMR titration data and computational modeling[8,16], we determined that CXCL4 and CXCL12 chemokines formed the heterodimer of CXC-type, in which the first beta-strand β1 from each chemokine monomer participated in the inter-monomer interface (Fig. 1a). We used this molecular model to generate an obligate, e.g., a non-dissociating CXCL4–CXCL12 heterodimer, termed OHD$_{4-12}$. To generate the OHD$_{4-12}$, we utilized the disulfide trapping strategy[17,30,31], because the inter-monomer interface of the CXC-type CXCL4–CXCL12 heterodimer is suitable for introducing cysteine amino acid residues for disulfide bond formation.

The rationale for amino acid residue selection for cysteine substitutions was as follows. First, CXCL4 and CXCL12 chemokines can form the CXC-type homodimers. Therefore, to avoid the formation of disulfide-linked homodimers, we excluded from consideration residues that directly face each other at the homodimer interface, i.e., E28 in CXCL4 and K27 in CXCL12 (Fig. 1b). For the same reason, we also excluded from consideration residues located next to E28 and K27, i.e., residues in positions 27 and 29 in CXCL4 and 26 and 28 in CXCL12. Next, we considered two pairs of residues located one residue apart from E28 and K27 and having side chains pointing in the same direction to facilitate the disulfide bond formation when substituted for cysteines. These residue pairs were S26-L29 and I30-H25 (the first listed residue is from CXCL4 and the second residue is from CXCL12). While these residues were still located at the heterodimer interface, they were sufficiently far from the symmetry axis to form disulfide-bonded homodimers. Finally, while either pair was suitable for cysteine substitution, we selected S26 in CXCL4 and L29 in CXCL12 (Fig. 1b) because at least serine-to-cysteine substitution was conservative and did not alter the charge state of the intermonomer interface.

CXCL4-S26C and CXCL12-L29C mutants were expressed and purified individually as detailed in the Methods section. To form the heterodimer, we mixed the mutants at a 1:1 molar ratio in phosphate buffer containing a catalytic amount of Cu^{2+} as an oxidizing agent[32]. After the incubation for 18 h at 4 °C, the OHD$_{4-12}$ was purified from the reaction mixture by size-exclusion chromatography. The elution time of the 15.7 kDa OHD$_{4-12}$ was approximately the same as of the 17 kDa myoglobin and smaller than of the 14.6 kDa lysozyme (Fig. 2a), indicating that the produced species had the correct molecular weight. Additionally, the Western Blot (WB) analysis in non-reducing (bands on the left) and reducing (bands on the right) conditions further verified the formation
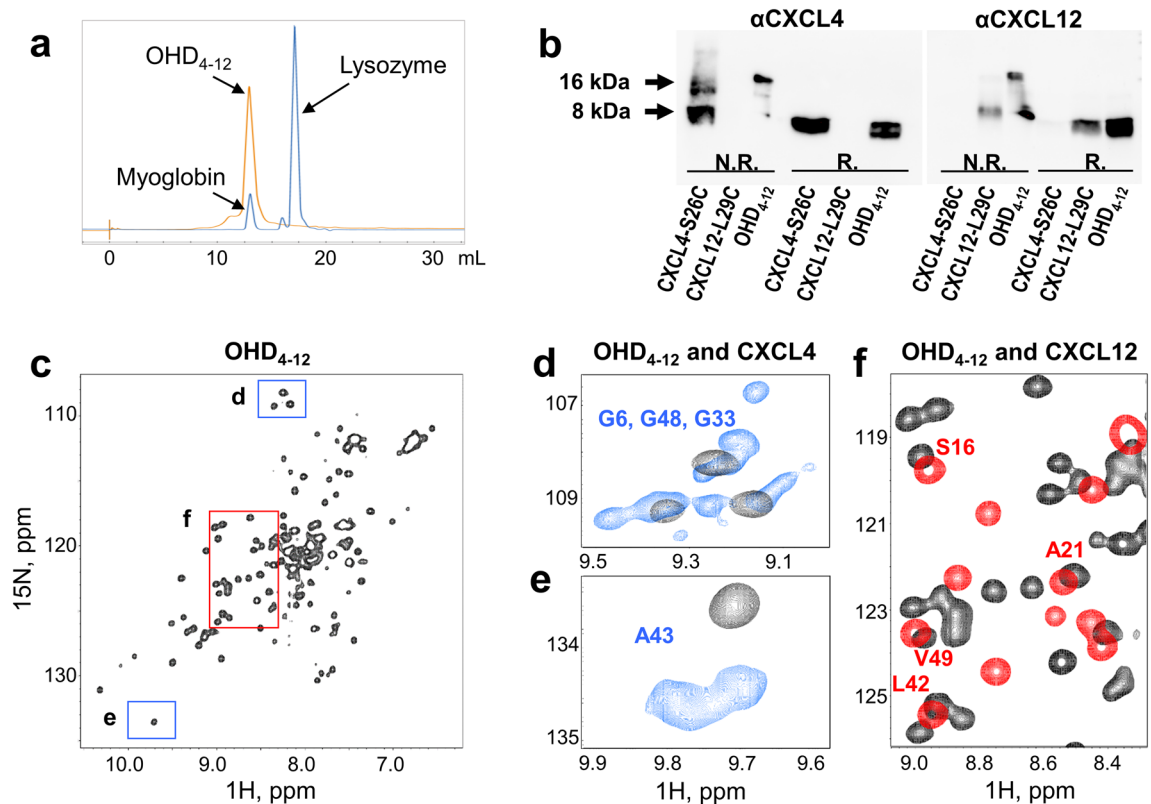
Figure 2. (**a**) Size-exclusion chromatograms. The elution profiles of lysozyme (14.4 kDa) and myoglobin (17 kDa) in blue and OHD_{4-12} (15.9 kDa) in orange are shown. (**b**) WB analysis in non-reduced (left bands, N.R.) and reduced (right bands, R.) conditions demonstrates the presence of OHD_{4-12} obtained following the mixing of CXCL4-S26C and CXCL12-L29C mutants in the presence of Cu^{2+} detected with anti-CXCL4 (αCXCL4) or anti-CXCL12 (αCXCL12) antibodies (see also Supplementary Fig. S1). (**c**) NMR spectroscopic analysis of OHD_{4-12} folding state. The 15N-HSQC NMR spectrum of the uniformly 15N-labeled 68 μM OHD_{4-12} in 90% H2O/10% D_2O at pH 6.9 in the presence of 20 mM NaCl, collected at 40 °C. (**d–f**) Expansions from the OHD_{4-12} spectrum overlaid with $CXCL4_{wt}$ (blue) and $CXCL12_{wt}$ (red) 15N-HSQC NMR spectra. Known signal assignments for CXCL4 and CXCL12 are indicated. The 15N-HSQC NMR spectrum of the uniformly 15N-labeled 150 μM CXCL4 in 90% H2O/10% D_2O at pH 5.0 in the presence of 20 mM NaCl was collected at 40 °C. The 15N-HSQC NMR spectrum of the uniformly 15N-labeled 51 μM CXCL12 in 20 MES buffer prepared with 90% H2O/10% D_2O at pH 6.8 was collected at 25 °C. The difference in experimental conditions was due to the difference in solubility properties of CXCL4 and CXCL12.

of the OHD_{4-12} with an expected molecular weight of ~ 16 kDa (Fig. 2b, the full gel is shown in Supplementary Fig. S1). Finally, the formation of the OHD_{4-12} was confirmed in co-immunoprecipitation (co-IP) experiments using antibodies specific to CXCL4 and CXCL12. The CXCL4-S26C or CXCL12-L29C fractions were first immunoprecipitated with magnetic microbeads coated with anti-CXCL4 or anti-CXCL12 antibodies and then detected using anti-CXCL12 antibodies, demonstrating the presence of the OHD_{4-12} heterodimer (Supplementary Fig. S2).

We then used NMR spectroscopy to assess the folding state of the OHD_{4-12}. The CXCL4-S26C and CXCL12-L29C mutants were individually uniformly 15N-enriched and used to produce the uniformly 15N-enriched OHD_{4-12}. The 15N-HSQC (heteronuclear single-quantum coherence) NMR spectrum of the 15N-OHD_{4-12} displayed well-dispersed cross-peaks, which confirmed the presence of a folded structure (Fig. 2c). The number of cross-peaks corresponded to the number of amino acids in the OHD_{4-12}, indicating the presence of a single heterodimer species. This simplified pattern contrasts the 15N-HSQC spectrum of 15N-enriched CXCL4, for which multiple resonances represent most amino acids due to the intermediate-to-slow exchange equilibrium between CXCL4 monomers, homodimers, and homotetramers on the NMR time scale and the asymmetry of CXCL4 homotetramer[15,33,34]. Figure 2d,e show representative expansions of overlaid 15N-HSQC spectra of 15N-CXCL4 (blue cross-peaks) and 15N-OHD_{4-12} (black cross-peaks). Unlike CXCL4, the CXCL12 chemokine produces the 15N-HSQC NMR spectrum, in which a single resonance represents each amino acid. Some heterodimer cross-peaks originating from the CXCL12 counterpart can be tracked by comparing the 15N-HSQC NMR spectra of the 15N-OHD_{4-12} (black cross-peaks) and 15N-CXCL12 (red cross-peaks). Some of these peaks are labeled in Fig. 2f, showing an expansion of the overlaid spectra of the OHD_{4-12} and CXCL12. Supplementary Fig. S3 provides the overlay of full 15N-HSQC NMR spectra of the OHD_{4-12}, CXCL12, and CXCL4 with known assignments for CXCL4 and CXCL12 labeled.
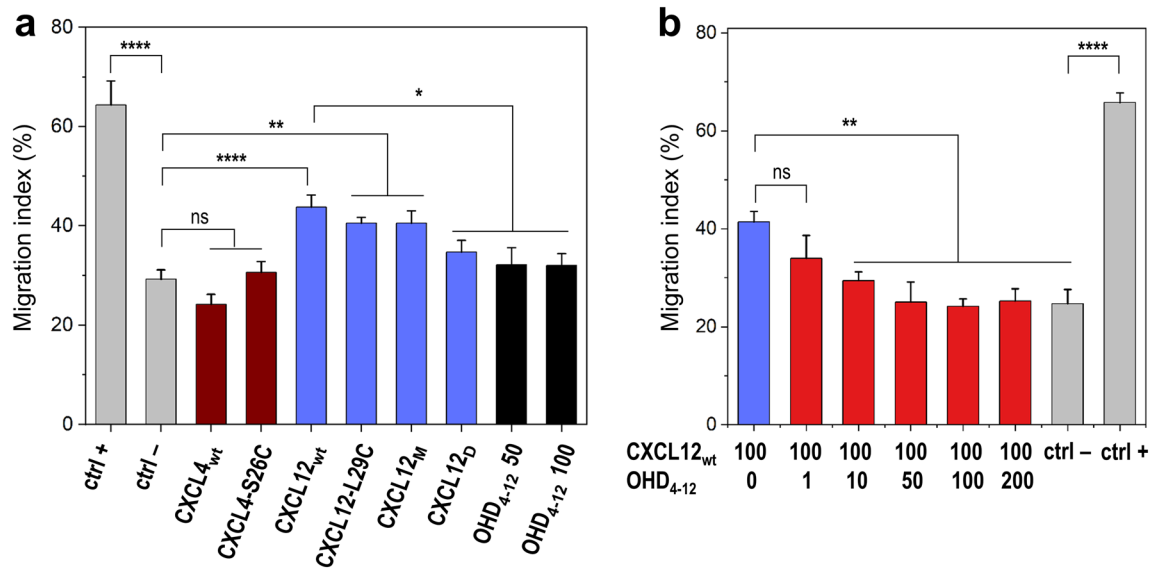
Figure 3. MDA-MB 231 breast cancer cells migration. (**a**) Migration of MDA-MB 231 cells treated with 100 nM of CXCL4$_{wt}$, its mutant CXCL4-S26C used as a CXCL4 counterpart to produce OHD$_{4-12}$, CXCL12$_{wt}$, its mutant CXCL12-L29C used as a CXCL12 counterpart to produce OHD$_{4-12}$, CXCL12 variants CXCL12$_M$ (obligate monomer) and CXCL12$_D$ (obligate dimer), and 50 or 100 nM of OHD$_{4-12}$. Negative and positive controls were 0 and 10% FBS. Migration index was determined as a percentage of wound healing in the absence of chemokine treatment at 0% FSB. (**b**) Competitive inhibition of CXCL12-driven migration of MDA-MB 231 cells by OHD$_{4-12}$ at concentrations ranging from 1 to 200 nM. The OHD$_{4-12}$ inhibits CXCL12-induced migration of MDA-MB 231 cells in a dose–response manner. The migration of cells treated with 100 nM CXCL12$_{wt}$ alone is shown for comparison. Negative and positive controls were as in panel (**a**). All presented data are means ± SEM (standard errors of the means) from n ≥ 3 independent experiments. *$p < 0.05$; **$p < 0.01$; ****$p < 0.0001$; analyzed by one-way ANOVA followed by a post-hoc Tukey multiple comparison test.

OHD$_{4-12}$ inhibits the CXCL12-induced migration of breast cancer MDA-MB-231 cells.

Next, we sought to determine whether the CXCL4–CXCL12 chemokine heterodimer is a biologically active species. Previously, we demonstrated that the addition of CXCL4 to CXCL12 chemokine led to the inhibition of CXCL12-induced migration of triple-negative MDA-MB-231 breast cancer cells in a wound-healing assay[16]. Here, we similarly assessed the effect of the OHD$_{4-12}$ on the migration of MDA-MB-231 cells. As expected, the wild-type CXCL12 (CXCL12$_{wt}$) and the mutant CXCL12-L29C, used to produce the disulfide-trapped heterodimer, induced the migration of MDA-MB-231 cells (Fig. 3a). We also observed the differential effect of the obligate CXCL12 monomer (CXCL12$_M$) and dimer (CXCL12$_D$) on cell migration[35] (Fig. 3a). Cell response to CXCL12$_M$ was comparable to the wild-type CXCL12$_{wt}$ and CXCL12-L29C, whereas CXCL12$_D$ had a lesser effect. In contrast to CXCL12, at the concentration used, the wild-type CXCL4$_{wt}$ and its mutant CXCL4-S26C, used to produce the disulfide-trapped heterodimer, did not significantly affect the MDA-MB-231 cell migration (Fig. 3a).

Several possible activities of the CXCL4–CXCL12 heterodimer, constructed from two chemokines with opposite effects on cell migration, can be expected: no effect or inhibition of cell migration as with CXCL4$_{wt}$ or CXCL4-S26C, notably or weakly enhanced cell migration as with CXCL12$_{wt}$, CXCL12-L29C, CXCL12$_M$ or CXCL12$_D$, and new activity[12,36]. Our data show that the OHD$_{4-12}$ alone has no significant effect on MDA-MB-231 cell migration at concentrations of 50 and 100 nM (Fig. 3a). However, when added to CXCL12, the OHD$_{4-12}$ inhibits the CXCL12-driven MDA-MB-231 cell migration at a concentration equivalent to 2:1, 1:1, and 1:2 (CXCL12:heterodimer) molar ratios (Fig. 3b).

Involvement of chemokine receptors CXCR4 and CXCR3 in the OHD$_{4-12}$ activity.

Two chemokine counterparts of the OHD$_{4-12}$, CXCL12, and CXCL4, bind receptors CXCR4 and CXCR7 (ACKR3) or CXCR3b, respectively[37–41]. Previously, we determined that MDA-MB-231 breast cancer cells strongly express CXCR4 and CXCR3b receptors[16]. The expression of the CXCR7 receptor on MDA-MB-231 cells is marginally low[42,43]. In our experimental setting, the percent of CXCR7 receptor expression on MDA-MB-231 cells was 1.6 ± 0.1, whereas the CXCR4 and CXCR3b expression was 23.5 ± 2.7 and 38.0 ± 0.2%, respectively (Supplementary Fig. S4). Accordingly, MDA-MB-231 breast cancer cells present a uniquely suitable model system for investigating the involvement of CXCR4 and CXCR3 receptors in the CXCL4–CXCL12 heterodimer signaling. Indeed, low expression of the CXCR7 receptor allows the assessment of the OHD$_{4-12}$ signaling through the CXCR4 receptor without CXCR7 interference, either as a CXCL12 scavenger[44,45] or through CXCR4-CXCR7 heterodimerization[46].

In highly invasive cells, such as MDA-MB-231 breast cancer cells, the binding of CXCL12 to CXCR4 activates multiple downstream signaling pathways, including calcium mobilization[47]. First, we verified that CXCL12$_{wt}$, CXCL12-L29C, CXCL12M, and CXCL12D, but not CXCL4-S26C or CXCL12$_{wt}$ mixed with the specific CXCR4 inhibitor AMD3100 led to the increase of cytoplasmic Ca^{2+} in MDA-MB-231 breast cancer cells (Supplementary
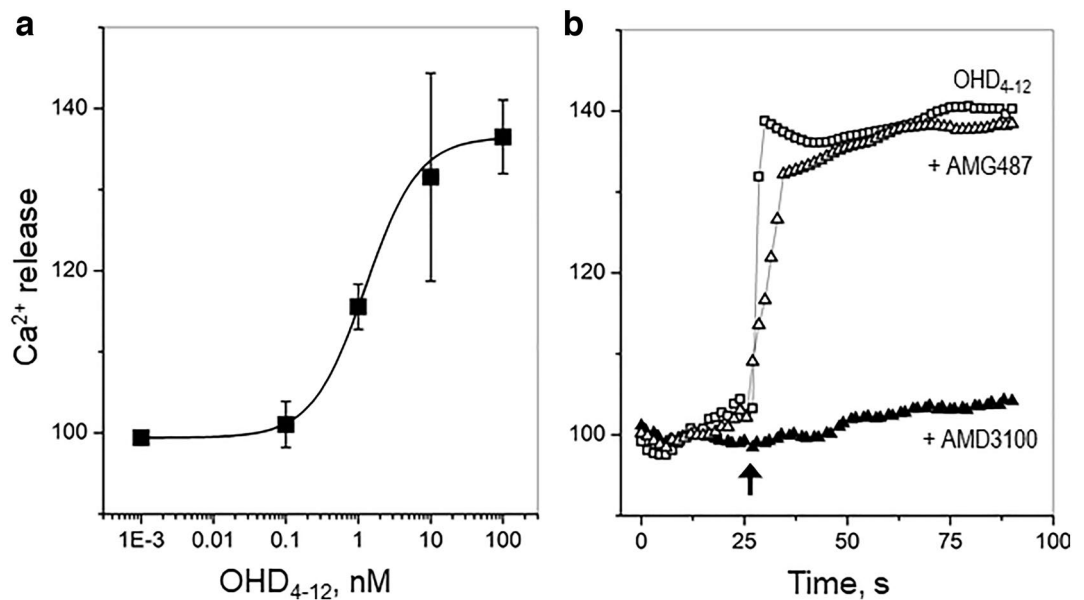
Figure 4. The cytoplasmic Ca^{2+} release in MDA-MB-231 breast cancer cells induced by OHD_{4-12}. (**a**) The dose–response curve of intracellular Ca^{2+} release induced by OHD_{4-12}. Solid line represents the best fit of experimental data using the logistic function. (**b**) The cytoplasmic Ca^{2+} release in MDA-MB-231 cells induced by 100 nM OHD_{4-12} (open squares). The arrow indicates the time-point of chemokine addition. The pre-incubation of cells with the CXCR4 antagonist AMD3100 (20 nM, solid triangles) inhibited, whereas the pre-incubation of cells with the CXCR3 antagonist AMG487 (5 nM, open triangles) had no effect on the OHD_{4-12}-induced intracellular Ca^{2+} release.

Fig. S5). Then, we tested the ability of the OHD_{4-12} to bind and activate the CXCR4 receptor by monitoring changes in cytoplasmic calcium (Ca^{2+} release) incubated with different amounts of the OHD_{4-12}. The addition of OHD_{4-12} to MDA-MB-231 cells induced a dose-dependent increase of cytoplasmic Ca^{2+} (Fig. 4a) with the half-maximal effective concentration (EC50) of 1.3 ± 0.1 nM. The addition of the specific CXCR4 inhibitor AMD3100 abrogated the Ca^{2+} release (Fig. 4b), confirming that the OHD_{4-12} activated the downstream signaling of the CXCR4 receptor. In contrast, the addition of the specific CXCR3 inhibitor AMG487 had no effect (Fig. 4b), demonstrating that the OHD_{4-12} does not activate those CXCR3 signaling pathways that lead to calcium mobilization at least at concentrations up to 100 nM.

Discussion

The formation of heterodimers by different chemokines is established experimentally, in in vitro and in vivo settings[6–9,11–13,15–17,19,22,23,25,31]. However, whether these heterodimers are biologically active species with unique functions or the response to chemokine mixtures is simply a combination of cell responses to individual chemokines remains debated and the mode of action of chemokine heterodimers remains to be determined. In this work, our primary goal was to determine whether the CXCL4–CXCL12 heterodimer possesses its own biological activity and, for the mechanistic insight, whether it can bind and activate receptors of chemokines forming the heterodimer.

The existence of the equilibrium of interconverting chemokines species in situ (i.e., reviewed in[28,48,49]) does not permit the investigation of cell response to chemokine heterodimers apart from chemokine monomers, homodimers, and, possibly, higher-order oligomers. Therefore, a powerful strategy to address this challenge is to use obligate, non-dissociating chemokine heterodimers in functional studies[12,17,31,36]. Here, we generated a new, obligate CXCL4–CXCL12 chemokine heterodimer, named OHD_{4-12}. The CXC-type arrangement of chemokine monomers forming the CXCL4–CXCL12 heterodimer[8,16] is particularly suitable for introducing cysteine substitutions at the intermonomer interface for disulfide bond formation. Therefore, we followed the disulfide-trapping strategy[17,30,31] for forming the OHD_{4-12}.

The CXCL4–CXCL12 heterodimer-forming chemokine pair was selected because of the high probability of forming heterodimers in vivo. Both chemokines are stored in platelets and released after platelet activation[29]. Indeed, previously we showed the physical interaction of CXCL4 and CXCL12 chemokines by co-immunoprecipitating them from human platelets[8]. Furthermore, the interaction with GAGs facilitates the accumulation and localization of chemokines in situ to establish gradients (e.g., reviewed in[4]), including CXCL12 and CXCL4. The GAG-binding of a few chemokine heterodimers was characterized[17,31] and it was also shown that binding to GAGs stabilized chemokine heterodimers[13]. Thus, it is plausible that the two heterodimer-forming chemokines dissociate from GAGs as a heterodimer, or remain close to each other to form a heterodimer, readily available for receptor binding. Further interest in CXCL4–CXCL12 heterodimer comes from the critical role of the CXCL12 chemokine and its receptor, CXCR4, in invasion, migration, and proliferation steps of tumor progression

in more than 75% of all cancers, including breast, ovarian, lung, colon, prostate, kidney, melanoma, brain, esophageal, pancreatic, and various forms of leukemia[50,51]. Indeed, organs with the highest levels of CXCL12 expression (lymph nodes, lung, liver, and bone marrow) are the most common sites of metastasis for breast cancer cells[51,52]. CXCL4 is abundant in platelets of healthy individuals. The levels of CXCL4 and CXCL12 can be further elevated in cancer patients[53,54] leading to micromolar concentrations at the tumor or metastasis site that could favor CXCL4–CXCL12 heterodimerization in vivo. Therefore, we tested the activity of the OHD_{4-12} on the migration of invasive MDA-MB-231 breast cancer cells. MDA-MB-231 are triple negative breast cancer cells extensively used in the investigation of therapeutic targets as well as mechanistic studies of cancer cell migration[55-57]. Although other cells, including different types of cancer cells, may trigger stronger than MDA-MB-231 cell migration responses[58], MDA-MB-231 cells uniquely express CXCR4 and CXCR3b but not CXCR7 ([16,42,43] and Supplementary Fig. S4). This feature makes MDA-MD-231 uniquely suitable for the investigation of CXCL12-CXCL4 heterodimer signaling.

Previously, we demonstrated that the addition of CXCL4 inhibited the CXCL12-induced migration of MDA-MB-231 cells in a dose-dependent manner and that a CXCL4-derived peptide mimicking the CXCL4–CXCL12 inter-monomer interface retained the inhibitory activity of CXCL4, suggesting that the CXCL4–CXCL12 heterodimer was at least partially responsible for the observed effect[16]. In the current study, by using the OHD_{4-12}, we explicitly proved that the CXCL4–CXCL12 heterodimer was an active species that inhibited the migration of MDA-MB-231 breast cancer cells driven by the CXCL12 chemokine and established the role of CXCL4–CXCL12 heterodimer in MDA-MB-231 breast cancer cell migration. In addition, our data support the paradigm that chemokine activity can be inhibited by CXC-type heterodimers[12].

Chemokines exert their functions by binding and activating GPCRs. In a generally applicable to all chemokines basic two-site model, chemokine signaling starts with the formation of an extensive protein-receptor interface between the unstructured N terminus of the receptor (chemokine recognition site 1—CRS1) and the globular core, N loop, and 40 s loop of the chemokine[59]. Subsequently, the flexible N-terminus of the chemokine interacts with other extracellular receptor residues and docks into a pocket within the transmembrane domain of the receptor (chemokine recognition site 2—CRS2), inducing conformational changes that lead to signaling[59-61]. The formation of the CXC-type CXCL4–CXCL12 heterodimer does not involve the N-terminus, N loop, or the 40 s loop of the chemokine ligand, and they remain available for interaction with the receptor (Fig. 1a)[16]. Our data show that the OHD_{4-12} can bind and activate the CXCL12's receptor CXCR4 with the EC50 of 1.3 ± 0.1 nM. The value of EC50, measured for Ca^{2+} release induced by the OHD_{4-12}, is comparable to EC50 values reported in the literature[30,62,63] or this work (1.0 ± 0.5 nM, Supplementary Fig. S5) for the wild-type CXCL12.

The observation that the OHD_{4-12} binds and activates the CXCR4 receptor is in accordance with previous observations that disulfide-trapped CXCL1-CXCL7 heterodimer binds and activates the CXCR2 receptor[17], whereas CC-type obligate CCL5-CCL17 heterodimer involves both corresponding receptors CCR4 and CCR5[12]. These observations suggest that chemokine heterodimers may act by involving receptors of both heterodimer-forming chemokines. Our data show that the addition of the specific CXCR4 inhibitor AMD3100 abrogates the OHD_{4-12}-induced Ca^{2+} release, whereas the addition of the specific CXCR3 inhibitor AMG487 does not (Fig. 4b), indicating that CXCR3 signaling pathways leading to calcium mobilization are not activated by 100 nM OHD_{4-12}. However, these data do not entirely exclude the involvement of the CXCR3 receptor. First, OHD_{4-12} may activate CXCR3 signaling pathways not tested in this work, such as activation of adenylyl cyclase activity[41]. Second, the lack of CXCR3-mediated Ca^{2+} release observed in this work may be due to significantly higher concentrations of OHD_{4-12} (i.e., its CXCL4 counterpart) required for the activation of CXCL4-CXCR3 Ca^{2+} signaling. Indeed, Korniejewska et al.[64] used 10 μM CXCL4, and Mueller et al.[65] reported that 500 nM CXCL4 was required to induce intracellular calcium flux in activated T cells. The 20-fold concentration discrepancy was proposed to be related to the difference in stimuli used for cell activation[64]. Further investigation will reveal whether the OHD_{4-12} can bind and activate the CXCR3 receptor.

The difference in effects of $CXCL12_M$ (e.g., the CXCL12-H25R mutant) and $CXCL12_D$ (disulfide-linked) on the migration of colon cancer HCT116 and HT29 and monocytic leukemia THP-1 cells was previously observed[30,35]. $CXCL12_D$ competitively blocked $CXCL12_{wt}$-induced cell migration and, in contrast to $CXCL12_M$, was not able to stimulate the migration of these cells at the concentration of 10 nM[35]. Our data parallel this result as we observe a reduced migration of MDA-MB-231 cells treated with 100 nM $CXCL12_D$ as compared to $CXCL12_{wt}$ or $CXCL12_M$ and CXCL12-L29C variants. The difference in $CXCL12_M$ and $CXCL12_D$ activity stems from different binding modes to the CXCR4 receptor[30,35,62]. In the case of $CXCL12_M$, the N-terminal domain of the CXCR4 receptor wraps around the chemokine and forms a beta-sheet with its first beta-strand β1, leading to an active signaling complex that promotes chemotaxis[35,62,66]. The lack of the $CXCL12_D$ chemotactic activity is caused by the inaccessibility of the β1 strand of the CXCL12 monomer for the interaction with the receptor because it participates in the inter-monomer contact with the β1 strand of an opposing CXCL12 monomer[30,62].

Similar to $CXCL12_D$, we observe no significant effect of the OHD_{4-12} on the migration of MDA-MB-231 breast cancer cells and the inhibition of the $CXCL12_{wt}$-induced MDA-MB-231 cell migration by the OHD_{4-12}. The design of the OHD_{4-12} (Fig. 1) requires that the β1 strand of the CXCL12 monomer in the CXCL4–CXCL12 heterodimer is involved in the inter-monomer interface with the CXCL4 monomer and has to be similarly inaccessible for the interactions with the CXCR4 receptor as in $CXCL12_D$. Thus, both the $CXCL12_D$ and the OHD_{4-12} may have a similar mode of receptor activation leading to cell migration. This observation may further extend to the CXCL4–CXCL12 heterodimers formed in vivo.

In summary, we present a new obligate heterodimer OHD_{4-12}, a tool for investigating the CXCL4–CXCL12 heterodimer functionalities in vitro or in vivo. Using the OHD_{4-12}, we demonstrate that it interrupts the CXCL12-driven migration of breast cancer cells, thus establishing the role of CXCL4–CXCL12 heterodimer in breast cancer and suggesting its utility for therapeutic advantage. Furthermore, our results on CXCR4 receptor activation

by the OHD_{4-12} provide the basis for further mechanistic studies of chemokine heterodimers and are likely to be broadly applicable to chemokine heterodimer-receptor interactions.

Methods

Protein expression and purification.

Plasmids with DNA encoding $CXCL4_{wt}$, $CXCL12_{wt}$ or CXCL4-S26C and CXCL12-L29C mutants inserted into pET-24d(+) vector (Novagen) were purchased from Genscript. Unlabeled or uniformly 15N-enriched proteins were expressed in BL21(DE3) pLysS E. coli bacteria (Novagen) grown in LB or M9 media, respectively, at 37 °C with shaking at 250 rpm in the presence of 60 μg/mL kanamycin. M9 medium was supplied with 15N-NH_4Cl (15N, 99%) (Cambridge Isotope Laboratories) as a sole source of nitrogen. Protein production was induced by the addition of IPTG (isopropyl β-D-1-thiogalactopyranoside) to the final concentration of 0.5 mM when the optical density of bacterial culture at 600 nm (OD_{600}) reached 0.6. After the addition of IPTG, bacteria were grown for 4 h at 37 °C and harvested by centrifugation for 30 min at 3000 rpm. Bacterial pellet was resuspended in the lysis buffer (3 ml per gram of pellet), contained 50 mM Tris, 1% Triton, 100 mM PMSF (phenylmethylsulfonyl fluoride), and 0.1% of beta-mercaptoethanol (BME), prepared at pH 8.0. Bacteria were disrupted by sonication (Branson Digital Sonifier) on ice at 40% amplitude for 2 s on/0.5 s off with breaks between cycles to prevent overheating. After sonication, bacteria lysates were centrifuged for 1 h at 20,000 rpm and 4 °C. All proteins expressed as inclusion bodies. Inclusion bodies were homogenized by stirring overnight at 4 °C in the extraction buffer prepared at pH 8.0 (12 ml per gram of pellet with inclusion bodies), containing 50 mM Tris, 8 M Urea, and 0.1% BME. Cell debris were removed by centrifugation at 20,000 rpm and 4 °C for 1 h, and the supernatant containing unfolded soluble proteins was used in subsequent purification steps.

The proteins were initially purified by cation exchange chromatography using the ÄKTA pure 25 M FPLC system and HiTrap SP/FF 16/10 column (Cytiva). $CXCL4_{wt}$, $CXCL12_{wt}$, and CXCL4-S26C proteins were eluted using a 0–100% gradient of elution buffer containing 100 mM Tris, 6 M urea, 2 M NaCl, pH 8.0. Following cation exchange chromatography, the refolding of $CXCL4_{wt}$, $CXCL12_{wt}$, and CXCL4-S26C was performed by 1:50 drop-wise dilution with constant stirring in 100 mM Tris buffer containing 10 mM cysteine and 1 mM cystine at pH 8.0. CXCL12-L29C was refolded on-column by gradually decreasing the concentration of urea from 8 to 1 M using 50 mM Tris buffer containing 10 mM reduced glutathione and 1 mM oxidized glutathione at pH 7.3. Following overnight incubation, the column was washed with 50 mM Tris buffer, pH 7.3, containing 50 mM NaCl. Folded CXCL12-L29C was eluted from the column with a 0–2 M gradient of NaCl. All refolded proteins were further purified by heparin affinity chromatography using HiPrep Heparin FF 16/10 column (Cytiva). The proteins were eluted in the 50 mM Tris buffer at pH 7.3 using a 0–2 M NaCl gradient. The $CXCL4_{wt}$ and CXCL4-S26C, eluting at high NaCl concentration, were sufficiently pure and were ready for subsequent experiments. The purity of $CXCL12_{wt}$ and CXCL12-L29C, eluting at ~ 0.3 M NaCl, was additionally improved by size-exclusion chromatography using HiPrep 26/60 Sepharcryl S-200 HR column (Cytiva) and 50 mM sodium phosphate buffer containing 150 mM sodium chloride at pH 7.0.

To form the disulfide-trapped heterodimer OHD_{4-12}, mutants CXCL4-S26C and CXCL12-L29C obtained after the heparin affinity chromatography step, were mixed at 1:1 molar ratio and dialyzed against 50 mM sodium phosphate buffer, containing 150 mM NaCl and 10 μM $CuCl_2$ at pH 7.0 for 18 h at 4 °C. Following the dialysis, the mixture was centrifuged to remove the precipitated proteins and the OHD_{4-12} was purified using HiTrap Heparin FF 16/10 column (Cytiva). The OHD_{4-12} eluted at 0.5–0.6 M of NaCl. The purity of OHD_{4-12} was polished by size-exclusion chromatography using a Superdex 75 Increase 10/300 GL column (Cytiva).

Obligate CXCL12 monomer ($CXCL12_M$) and dimer ($CXCL12_D$) were a gift from Protein Foundry, LLC.

Western blot and co-immunoprecipitation analyses.

Chemokine mixtures or the OHD_{4-12} were electrophoretically separated in non-denaturing or denaturing conditions using 16.5% polyacrylamide gel and then transferred to 0.2 μm nitrocellulose membrane using a semi-transfer apparatus (Biorad). Membranes were blocked in Tris-buffered saline containing 0.1% Tween-20 and 5% non-fat milk at 4 °C and incubated with the primary anti-CXCL4 and anti-CXCL12 antibodies (MAB7952 and MAB310, respectively, R&D systems) overnight. The membranes were then incubated with species-specific horseradish-peroxidase-(HRP)-conjugated secondary antibodies (#31450, ThermoFisher). Following the incubation with ECL substrate (BioRad), the presence of specific proteins was determined based on chemiluminescence detected using a ChemiDoc Imaging System (BioRad). For co-IP analysis, chemokine mixtures were incubated with magnetic microbeads pre-coated with mouse anti-CXCL4 or anti-CXCL12 antibodies (R&D Systems) at 4 °C for 2 h. After incubation, microbeads were magnetically bound and washed to remove the unbound fractions. After elution, the Western blot analysis of the immune-precipitated samples was performed using goat anti-CXCL12 monoclonal antibodies (R&D Systems).

NMR spectroscopy.

15N-CXCL4 was prepared at the concentration of 150 μM in 90% H_2O/10% D_2O in the presence of 20 mM of NaCl at pH 5.0. 15N-CXCL12 and 15N-OHD_{4-12} (both counterparts were 15N-labeled) were prepared at concentrations 129 and 68 μM, respectively, in 90% H_2O/10% D_2O in the presence of 20 mM of NaCl at pH 6.9. The two-dimensional 15N-HSQC (heteronuclear single quantum coherence) spectrum of $CXCL4_{wt}$ was recorded on the Bruker Avance 950 MHz spectrometer at David H. Murdock Institute (Kannapolis, NC). 15N-HSQC spectra of $CXCL12_{wt}$ and OHD_{4-12} were recorded on the Bruker Avance III 700 MHz NMR spectrometer equipped with a helium-cooled cryoprobe at METRIC, North Carolina State University. All spectra were recorded at 40 °C.

Cell migration. MDA-MB 231 breast cancer cells (ATCC) were cultured in DMEM/F12 media (Corning) supplemented with 10% FBS (Atlanta Biologics), ʟ-glutamine, Amphotericin B and Gentamycin (Corning). Following an overnight coating with Collagen type I (12 µg/cm^2, BD Biosciences) at 37 °C with 5% CO_2 and > 85% humidity and washes of the unbound Collagen I with sterile PBS, 96-well tissue culture plates (Greiner) were seeded (4×10^5 cells/well) with MDA-MB 231 cell suspension in culture media. Cells were grown to confluence and then incubated overnight with fresh media without FBS (0%). The confluent MDA-MB 231 cell monolayers were then scratched using a sterile pipet tip and the wells washed to remove non-adherent cells. Thereafter, cells were incubated with various chemokines and overlapping microphotographs encompassing the entire area of each scratch/wound were taken at the start of the treatment and following the incubation for 9 h using an IX71 Olympus microscope equipped with a DP70 camera and the associated software (Olympus). Overlapping microphotographs were stitched together, and the area of the wound was determined using ImageJ software (NIH). After normalization to the area measured at time 0, results were expressed as percentage of wound healing. Differences between treatments were tested by ANOVA and individual treatment compared through post-hoc Tukey tests with a priori significance threshold set at $p < 0.05$.

Calcium release. MDA-MB 231 breast cancer cells (ATCC) were seeded at 4×10^5 cells in 100 µL per well on 96-well tissue culture plates (Greiner) and grown to confluence. After 48 h, cells were starved in serum-free media for 6 h and then incubated (45 min, 37 °C) with the Ca^{2+} intracellular indicator Fura-2 (2 µM). Cells were washed with phosphate buffered saline (PBS). Following injections of increasing concentrations of chemokines (0–250 nM), variations in cytoplasmic Ca^{2+} were measured every 1.5 s for up to 60 s by detecting the 510 nm fluorescence emission ratio following excitation at 340 nm and 380 nm, respectively, using the ID5 plate fluorescence reader (Molecular Device). Background fluorescence was measured for 30 s prior to the addition of chemokines. Fluorescent signals were subsequently normalized to the average background reading.

Data availability
All data that support the findings of this study are included in the article.

References
1. Gerard, C. & Rollins, B. J. Chemokines and disease. *Nat. Immunol.* **2**, 108–115 (2001).
2. Raman, D., Sobolik-Delmaire, T. & Richmond, A. Chemokines in health and disease. *Exp. Cell Res.* **317**, 575–589 (2011).
3. Allen, S. J., Crown, S. E. & Handel, T. M. Chemokine: Receptor structure, interactions, and antagonism. *Annu. Rev. Immunol.* **25**, 787–820 (2007).
4. Proudfoot, A. E. I., Johnson, Z., Bonvin, P., & Handel, T. M. Glycosaminoglycan interactions with chemokines add complexity to a complex system. *Pharmaceuticals (Basel).* **10**, 70-95(2017).
5. Guan, E., Wang, J. & Norcross, M. A. Identification of human macrophage inflammatory proteins 1alpha and 1beta as a native secreted heterodimer. *J. Biol. Chem.* **276**, 12404–12409 (2001).
6. Venetz, D. *et al.* Perivascular expression of CXCL9 and CXCL12 in primary central nervous system lymphoma: T-cell infiltration and positioning of malignant B cells. *Int. J. Cancer* **127**, 2300–2312 (2010).
7. Paoletti, S. *et al.* A rich chemokine environment strongly enhances leukocyte migration and activities. *Blood* **105**, 3405–3412 (2005).
8. Carlson, J., Baxter, S. A., Dreau, D. & Nesmelova, I. V. The heterodimerization of platelet-derived chemokines. *Biochim. Biophys. Acta* **1834**, 158–168 (2013).
9. Koenen, R. R. *et al.* Disrupting functional interactions between platelet chemokines inhibits atherosclerosis in hyperlipidemic mice. *Nat. Med.* **15**, 97–103 (2009).
10. Giri, J., Das, R., Nylen, E., Chinnadurai, R. & Galipeau, J. CCL2 and CXCL12 derived from mesenchymal stromal cells cooperatively polarize IL-10+ tissue macrophages to mitigate gut injury. *Cell Rep.* **30**(1923–1934), e1924 (2020).
11. von Hundelshausen, P. *et al.* Heterophilic interactions of platelet factor 4 and RANTES promote monocyte arrest on endothelium. *Blood* **105**, 924–930 (2005).
12. von Hundelshausen, P., Agten, S. M., Eckardt, V., Blanchet, X., Schmitt, M. M., Ippel, H., Neideck, C., Bidzhekov, K., Leberzammer, J., Wichapong, K., Faussner, A., Drechsler, M., Grommes, J., van Geffen, J. P., Li, H., Ortega-Gomez, A., Megens, R. T., Naumann, R., Dijkgraaf, I., Nicolaes, G. A., Doring, Y., Soehnlein, O., Lutgens, E., Heemskerk, J. W., Koenen, R. R., Mayo, K. H., Hackeng, T. M., & Weber, C. (2017) Chemokine interactome mapping enables tailored intervention in acute and chronic inflammation. *Sci. Transl. Med.* **9**(384), eaah6650 (2017).
13. Crown, S. E., Yu, Y., Sweeney, M. D., Leary, J. A. & Handel, T. M. Heterodimerization of CCR2 chemokines and regulation by glycosaminoglycan binding. *J. Biol. Chem.* **281**, 25438–25446 (2006).
14. Dudek, A. Z. *et al.* Platelet factor 4 promotes adhesion of hematopoietic progenitor cells and binds IL-8: novel mechanisms for modulation of hematopoiesis. *Blood* **101**, 4687–4694 (2003).
15. Nesmelova, I. V. *et al.* Platelet factor 4 and interleukin-8 CXC chemokine heterodimer formation modulates function at the quaternary structural level. *J. Biol. Chem.* **280**, 4948–4958 (2005).
16. Nguyen, K. T. P. *et al.* CXCL12–CXCL4 heterodimerization prevents CXCL12-driven breast cancer cell migration. *Cell Signal* **66**, 109488 (2020).
17. Brown, A. J., Joseph, P. R., Sawant, K. V., & Rajarathnam, K. Chemokine CXCL7 Heterodimers: Structural Insights, CXCR2 Receptor Function, and Glycosaminoglycan Interactions. *Int. J. Mol. Sci.* **18**, 748-64 (2017).
18. Gouwy, M. *et al.* The unique property of the CC chemokine regakine-1 to synergize with other plasma-derived inflammatory mediators in neutrophil chemotaxis does not reside in its NH2-terminal structure. *Mol. Pharmacol.* **62**, 173–180 (2002).
19. Gouwy, M., Struyf, S., Catusse, J., Proost, P. & Van Damme, J. Synergy between proinflammatory ligands of G protein-coupled receptors in neutrophil activation and migration. *J. Leukoc. Biol.* **76**, 185–194 (2004).
20. Struyf, S. *et al.* Chemokines synergize in the recruitment of circulating neutrophils into inflamed tissue. *Eur. J. Immunol.* **35**, 1583–1591 (2005).
21. Broxmeyer, H. E. *et al.* Comparative analysis of the human macrophage inflammatory protein family of cytokines (chemokines) on proliferation of human myeloid progenitor cells. Interacting effects involving suppression, synergistic suppression, and blocking of suppression. *J. Immunol.* **150**, 3448–3458 (1993).

22. Kuscher, K. *et al.* Synergy-inducing chemokines enhance CCR2 ligand activities on monocytes. *Eur. J. Immunol.* **39**, 1118–1128 (2009).
23. Gouwy, M. *et al.* Synergy between coproduced CC and CXC chemokines in monocyte chemotaxis through receptor-mediated events. *Mol. Pharmacol.* **74**, 485–495 (2008).
24. Zwijnenburg, P. J. *et al.* CXC-chemokines KC and macrophage inflammatory protein-2 (MIP-2) synergistically induce leukocyte recruitment to the central nervous system in rats. *Immunol. Lett.* **85**, 1–4 (2003).
25. Sebastiani, S., Danelon, G., Gerber, B. & Uguccioni, M. CCL22-induced responses are powerfully enhanced by synergy inducing chemokines via CCR4: Evidence for the involvement of first beta-strand of chemokine. *Eur. J. Immunol.* **35**, 746–756 (2005).
26. Grommes, J. *et al.* Disruption of platelet-derived chemokine heteromers prevents neutrophil extravasation in acute lung injury. *Am. J. Respir. Crit. Care Med.* **185**, 628–636 (2012).
27. Salanga, C. L. & Handel, T. M. Chemokine oligomerization and interactions with receptors and glycosaminoglycans: the role of structural dynamics in function. *Exp. Cell Res.* **317**, 590–601 (2011).
28. Miller, M. C., and Mayo, K. H. Chemokines from a structural perspective. *Int. J. Mol. Sci.* **18**. 2088-2104 (2017).
29. Chatterjee, M. *et al.* Distinct platelet packaging, release, and surface expression of proangiogenic and antiangiogenic factors on different platelet stimuli. *Blood* **117**, 3907–3911 (2011).
30. Veldkamp, C. T. *et al.* Structural basis of CXCR4 sulfotyrosine recognition by the chemokine SDF-1/CXCL12. *Sci. Signal.* **1**, 4 (2008).
31. Sepuru, K. M. & Rajarathnam, K. Structural basis of a chemokine heterodimer binding to glycosaminoglycans. *Biochem. J.* **478**, 1009–1021 (2021).
32. Merkley, N., Barber, K. R. & Shaw, G. S. Ubiquitin manipulation by an E2 conjugating enzyme using a novel covalent intermediate. *J. Biol. Chem.* **280**, 31732–31738 (2005).
33. Chen, M. J. & Mayo, K. H. Human platelet factor 4 subunit association/dissociation thermodynamics and kinetics. *Biochemistry-Us* **30**, 6402–6411 (1991).
34. Mayo, K. H. *et al.* NMR solution structure of the 32-kDa platelet factor 4 ELR-motif N-terminal chimera: a symmetric tetramer. *Biochemistry-Us* **34**, 11399–11409 (1995).
35. Drury, L. J. *et al.* Monomeric and dimeric CXCL12 inhibit metastasis through distinct CXCR4 interactions and signaling pathways. *Proc. Natl. Acad. Sci. USA* **108**, 17655–17660 (2011).
36. Agten, S. M. *et al.* Probing functional heteromeric chemokine protein-protein interactions through conformation-assisted oxime ligation. *Angew. Chem. Int. Ed. Engl.* **55**, 14963–14966 (2016).
37. Bleul, C. C. *et al.* The lymphocyte chemoattractant SDF-1 is a ligand for LESTR/fusin and blocks HIV-1 entry. *Nature* **382**, 829–833 (1996).
38. Oberlin, E. *et al.* The CXC chemokine SDF-1 is the ligand for LESTR/fusin and prevents infection by T-cell-line-adapted HIV-1. *Nature* **382**, 833–835 (1996).
39. Balabanian, K. *et al.* The chemokine SDF-1/CXCL12 binds to and signals through the orphan receptor RDC1 in T lymphocytes. *J. Biol. Chem.* **280**, 35760–35766 (2005).
40. Burns, J. M. *et al.* A novel chemokine receptor for SDF-1 and I-TAC involved in cell survival, cell adhesion, and tumor development. *J. Exp. Med.* **203**, 2201–2213 (2006).
41. Lasagni, L. *et al.* An alternatively spliced variant of CXCR3 mediates the inhibition of endothelial cell growth induced by IP-10, Mig, and I-TAC, and acts as functional receptor for platelet factor 4. *J. Exp. Med.* **197**, 1537–1549 (2003).
42. Hattermann, K. *et al.* Effects of the chemokine CXCL12 and combined internalization of its receptors CXCR4 and CXCR7 in human MCF-7 breast cancer cells. *Cell Tissue Res.* **357**, 253–266 (2014).
43. Salazar, N. *et al.* The chemokine receptor CXCR7 interacts with EGFR to promote breast cancer cell proliferation. *Mol. Cancer* **13**, 198 (2014).
44. Boldajipour, B. *et al.* Control of chemokine-guided cell migration by ligand sequestration. *Cell* **132**, 463–473 (2008).
45. Naumann, U. *et al.* CXCR7 functions as a scavenger for CXCL12 and CXCL11. *PLoS ONE* **5**, e9175 (2010).
46. Levoye, A., Balabanian, K., Baleux, F., Bachelerie, F. & Lagane, B. CXCR7 heterodimerizes with CXCR4 and regulates CXCL12-mediated G protein signaling. *Blood* **113**, 6085–6093 (2009).
47. Holland, J. D. *et al.* Differential functional activation of chemokine receptor CXCR4 is mediated by G proteins in breast cancer cells. *Cancer Res.* **66**, 4117–4124 (2006).
48. Weber, C. & Koenen, R. R. Fine-tuning leukocyte responses: towards a chemokine "interactome". *Trends Immunol.* **27**, 268–273 (2006).
49. Wang, X., Sharp, J. S., Handel, T. M. & Prestegard, J. H. Chemokine oligomerization in cell signaling and migration. *Prog. Mol. Biol. Transl. Sci.* **117**, 531–578 (2013).
50. Cojoc, M. *et al.* Emerging targets in cancer management: Role of the CXCL12/CXCR4 axis. *Onco. Targets Ther.* **6**, 1347–1361 (2013).
51. Ben-Baruch, A. Organ selectivity in metastasis: Regulation by chemokines and their receptors. *Clin. Exp. Metastasis* **25**, 345–356 (2008).
52. Zlotnik, A. Involvement of chemokine receptors in organ-specific metastasis. *Contrib. Microbiol.* **13**, 191–199 (2006).
53. Peterson, J. E. *et al.* VEGF, PF4 and PDGF are elevated in platelets of colorectal cancer patients. *Angiogenesis* **15**, 265–273 (2012).
54. Dabrowska, E. *et al.* Possible diagnostic application of CXCL12 and CXCR4 as tumor markers in breast cancer patients. *Anticancer Res.* **40**, 3221–3229 (2020).
55. Lehmann, B. D. *et al.* Identification of human triple-negative breast cancer subtypes and preclinical models for selection of targeted therapies. *J. Clin. Invest.* **121**, 2750–2767 (2011).
56. Chavez, K. J., Garimella, S. V. & Lipkowitz, S. Triple negative breast cancer cell lines: one tool in the search for better treatment of triple negative breast cancer. *Breast Dis.* **32**, 35–48 (2010).
57. Wang, Y., Li, L., Wang, H., Li, J. & Yang, H. Silencing TGIF suppresses migration, invasion and metastasis of MDAMB231 human breast cancer cells. *Oncol. Rep.* **39**, 802–808 (2018).
58. Dai, X., Cheng, H., Bai, Z. & Li, J. Breast cancer cell line classification and its relevance with breast tumor subtyping. *J. Cancer* **8**, 3131–3141 (2017).
59. Crump, M. P. *et al.* Solution structure and basis for functional activity of stromal cell-derived factor-1; dissociation of CXCR4 activation from binding and inhibition of HIV-1. *EMBO J.* **16**, 6996–7007 (1997).
60. Gustavsson, M. *et al.* Structural basis of ligand interaction with atypical chemokine receptor 3. *Nat. Commun.* **8**, 14135 (2017).
61. Wescott, M. P. *et al.* Signal transmission through the CXC chemokine receptor 4 (CXCR4) transmembrane helices. *Proc. Natl. Acad. Sci. USA* **113**, 9928–9933 (2016).
62. Ziarek, J. J., Kleist, A. B., London, N., Raveh, B., Montpas, N., Bonneterre, J., St-Onge, G., DiCosmo-Ponticello, C. J., Koplinski, C. A., Roy, I., Stephens, B., Thelen, S., Veldkamp, C. T., Coffman, F. D., Cohen, M. C., Dwinell, M. B., Thelen, M., Peterson, F. C., Heveker, N., and Volkman, B. F. Structural basis for chemokine recognition by a G protein-coupled receptor and implications for receptor activation. *Sci. Signal.* **10**(471):eaah5756 (2017).
63. Kufareva, I. *et al.* Stoichiometry and geometry of the CXC chemokine receptor 4 complex with CXC ligand 12: Molecular modeling and experimental validation. *Proc. Natl. Acad. Sci. USA* **111**, E5363-5372 (2014).

64. Korniejewska, A., McKnight, A. J., Johnson, Z., Watson, M. L. & Ward, S. G. Expression and agonist responsiveness of CXCR3 variants in human T lymphocytes. *Immunology* **132**, 503–515 (2011).
65. Mueller, A. *et al.* CXCL4-induced migration of activated T lymphocytes is mediated by the chemokine receptor CXCR3. *J. Leukoc. Biol.* **83**, 875–882 (2008).
66. Stephens, B. S., Ngo, T., Kufareva, I., and Handel, T. M. Functional anatomy of the full-length CXCR4-CXCL12 complex systematically dissected by quantitative model-guided mutagenesis. *Sci. Signal.* **13**(640):eaay5024 (2020).

Author contributions

Conceptualization, D.D. and I.V.N.; Data acquisition and analysis, K.T.P.N., D.D., and I.V.N.; Data interpretation, K.T.P.N., B.V., D.D., and I.V.N.; Writing, review, and editing, K.T.P.N., B.V., D.D., I.V.N.

Competing interests

The authors declare no competing interests.

Additional information

Supplementary Information The online version contains supplementary material available at https://doi.org/10.1038/s41598-022-21651-0.

Correspondence and requests for materials should be addressed to I.V.N.

Reprints and permissions information is available at www.nature.com/reprints.

Publisher's note Springer Nature remains neutral with regard to jurisdictional claims in published maps and institutional affiliations.